Quantifying Collisional Energies within an Ion Trap Mass Spectrometer by LabVIEW
Simulation

Kyser D. Seaney

Faculty Mentors: Michael P. Grubb, Callie A. Cole

Fort Lewis College

Abstract

The energetics involved in chemical reactions and the bond energies of ions are of fundamental importance to the field of chemistry. Conventional methods of collision induced dissociation (CID) within an ion trap mass spectrometer provide invaluable structural information on the ions in question. However, the energy imparted to the ions following repeated collisions with a neutral gas often remains ambiguous and unexplored. These energies are often simply represented by a unit-less quantity (such as normalized collisional energy, NCE %) instead of an absolute energy unit. In an effort to clarify this ambiguity, we herein present a LabVIEW simulation combined with mass spectrometry experiments which will allow both experimentalists and theoretical chemists alike to develop a more intuitive understanding of the collision energetics within an ion trap mass spectrometer. An experimental calibration of collision energy is conducted by performing CID on a series of ions with well-known bond energies. Next, a LabVIEW simulation is implemented and compared to the experimental observations to test its accuracy. The simulation is developed through the derivation of the two dimensional position equations from the Mathieu potential differential equations, which are subsequently solved through Velocity Verlet step integration. The collisional energy distributions may be quantified from the velocity distributions of the simulated ion trajectories. The collisional energy distribution calculated the most probable energy of collisions within 8.5% of the published bond energy metrics. Herein we present an efficient method for understanding the collision energetics within an ion trap mass spectrometer during CID is presented.

Keywords: Collision-Induced Dissocaition, Ion Trap Mass Spectrometer, Collisional-Energy Distribution, Ion Trajectory, Velocity Probability Distribution

Introduction

Collision induced dissociation (CID) mass spectrometry is a vital analytical technique used for identifying reactive sites on lipids and proteins,[1,2] isolating natural product fragments,[3] structural characterization of inorganic molecules,[4] structural identification of organic compounds,[5,6] and determining possible molecular transformations in astrochemistry[7,8] making it useful across many subdisciplines of chemistry. While the information it provides deems valuable, published scientific works often lack a quantitative measurement for the energy imparted to the parent ion during collisions. Instead, a unitless measurement is recorded as normalized collisional energy percent (NCE %). [1-8] Determining energy barriers proves essential for understanding chemical processes and, therefore, necessary for all subfields of chemistry. Previous methods for experimentally ascertaining enthalpies of formation for molecules involved constructing calibration curves relating the appearance NCE % to the known bond energy.[9,10] The appearance NCE % is the point at which the fragment molecule is detectable determined from linear extrapolation of the abundance graphs.[9,10] An example of these molecules is shown in **Figure 1**. While useful, this extrapolation does not give insight into the actual energies imparted to the parent ion. The appearance energy corresponds to the most energetic collisions in the trap or the tail end of the energy distributions. Therefore, we construct a calibration curve herein that relates a different NCE

% to the most probable energy of each collision. This NCE % is then assigned a literature bond energy.[12-18]
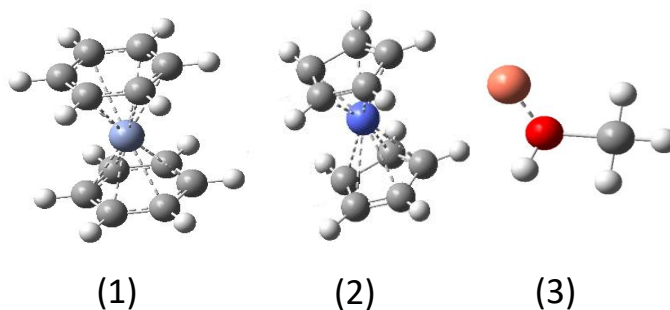

Figure 1. Several of the metal-ligand complexes under analysis are shown here: (1) bis(benzene)chromium(0), (2) bis(cyclopentadienyl)cobalt(II), and (3) methanol copper(I) complex.

This new NCE % is set at the point at which the fragment peak reaches half of its maximum relative abundance. This is a more accurate representation of the energetics involved in the system due to half of the collisions having an energy $\geq$ the bond energies of the atoms within a molecule. To further verify this proposed energy assignment, a simulation of the ion trajectories within the ion trap is constructed using LabVIEW. This is achieved by deriving the acceleration of the ion from the Mathieu potential differential equations.[11] The position is then determined by Velocity Verlet step integration. From the simulation, the collisional energy distributions between an ion and helium atom are derived from experimental parameters such as AC voltage, DC voltage, and the RF frequency of the trap. Simulations of ion trajectories within the trap have been created in previous studies.[11] However, these publications did not derive the velocity distributions of the ion, as we have done herein. Without the velocity distribution, energy distributions of collisions within the ion trap cannot be determined.[11] From the collisional energy distributions of the ion and helium atom, the most probable energy imparted on the ion is quantifiable. This calculated energy is checked against the experimental data acquired and previously reported bond energy values to determine the accuracy of the method. A method is provided for obtaining the actual collisional energy distributions between the parent ion and helium atom within any ring ion trap; this gives insight into the collisional energies within the trap for experimental and theoretical chemists performing CID mass spectrometry experiments.

Method

Experimental
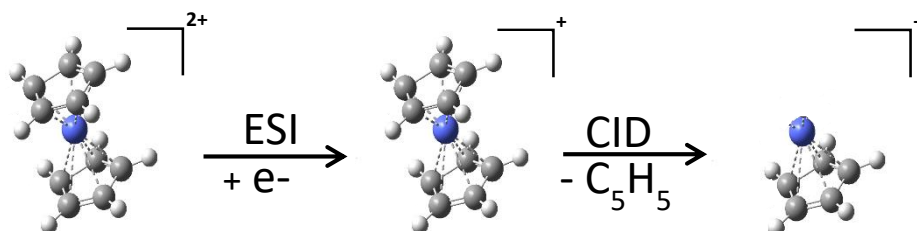
Scheme 1. The interactions that a cyclopentadienyl complex undergoes throughout the course of electrospray ionization (ESI) and collision induced dissociation (CID). ESI produces a singly charged cation that is accelerated into an ion trap mass spectrometer. Upon entering the ion trap, the ion is accelerated by an electric potential and fragmentation occurs through collisions with multiple helium atoms.

Various saturated solutions are prepared for ion generation by separately dissolving copper(I) bromide, bis- (benzene)chromium(0), bis(cyclopentadienyl)nickel(II), bis(cyclopentadienyl)chromium(II), bis(cyclopentadienyl)cobalt(II), bis(cyclopentadienyl)iron(II), potassium(I) glycinate, and glycine in 1:1 HPLC grade H_2O and methanol solvents. Aliquots (500 μL) of these $\sim 10^{-4}$ M solutions are introduced into an electrospray ionization (ESI) source ranging from 4-6.5 kV, at a rate of $10 \frac{\mu L}{min}$. Ion generation of the solutions is achieved by the ESI source and the free gas-phase ions are directed to the quadrupole and octupole mass spectrometers via the heated ion transfer tube. The charged ion beam is directed to the ion trap by the quadrupole and octupole mass spectrometers. Thermalization of the ions is achieved through collisions with helium gas particles. A schematic of the entire mass spectrometer is shown in **Figure 2**. Once a signal of the parent molecule is observed, the signal to noise ratio is optimized using LCQ Tune Software. Upon achieving the maximum signal to noise ratio, the normalized collisional energy (NCE%) is increased by 0.5% every second. The intensity of the parent molecule and fragment are recorded at each step. Once the parent molecule drops below 10^2 ion counts and the fragment peak in question reaches its maximum, the process is terminated. The data gathered is transferred to a spreadsheet program where the intensities of the peaks are normalized and plotted against NCE%. The NCE% at which the fragment peak reaches half the normalized intensity is recorded and assigned a bond dissociation energy obtained from the literature.[12-18] These data pairs are plotted and a calibration curve is generated.
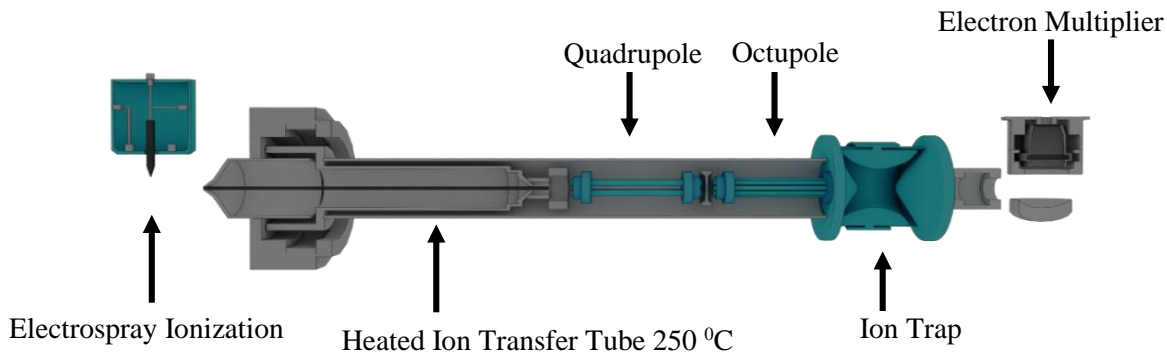
Figure 2. A schematic of the LCQ Deca XP Plus ion trap used in the collision induced dissociation experiments is shown above.

Simulation

A 2D simulation of the ion trajectories is created using LabVIEW software. This is done using the acceleration potentials of an ion trap, equation (2) and (3), derived from the Mathieu potential energy equation (1).[11]

$$\phi = \left(U + Vcos(\Omega t)\right) \tag{1}$$

$$a(t)_{x,y} = -\frac{qe}{m}\left(\frac{\phi}{r_0^2}\right)(x(t), y(t)) \tag{2}$$

$$a(t)_z = -\frac{2qe}{m}\left(\frac{\phi}{r_0^2}\right)z(t) \tag{3}$$

U represents the DC voltage, V is AC voltage, Ω is the angular momentum (Hz), m is mass of ion (kg), q represents the charge of the ion, e is the elementary charge (C), x(t) or y(t) and z(t) define the position (m), and r_0 corresponds to the radius of trap (m). These variables are entered into the program along with the initial velocity in the x, y, and z directions along with their initial positions. From the acceleration, the position of the particle is determined by step integration.

$$x(t_0 + \Delta t) = x(t_0) + v(t_o)\Delta t + \frac{1}{2}a(t_0)\Delta t^2 \tag{4}$$

$$a(t_0 + \Delta t)_x = x(t_0 + \Delta t)\frac{-qe}{m}\frac{(U+Vcos(\Omega(t_0+\Delta t))}{r_0^2} \tag{5}$$

$$v(t_0 + \Delta t)_x = \frac{1}{2}(a(t_0 + \Delta t) + a(t_0))\Delta t + v(t_o) \tag{6}$$

The position of the particle is determined initially through equation (4) using the initial velocity and position inputs. The acceleration is calculated by equations (2) or (3) depending on the

dimension being solved for. Once the position has been calculated from equation (4), the new acceleration is calculated as a result of equation (5). The new velocity is computed from equation (6) by the new acceleration calculated from equation (5). The circular step integration continues again, starting at equation (4). The x and z parametric position values are plotted against each other over time, displaying the trajectory of the ions as points. This leads to accurate projections of the trajectories in two dimensional space, as shown in **Figure 3.**
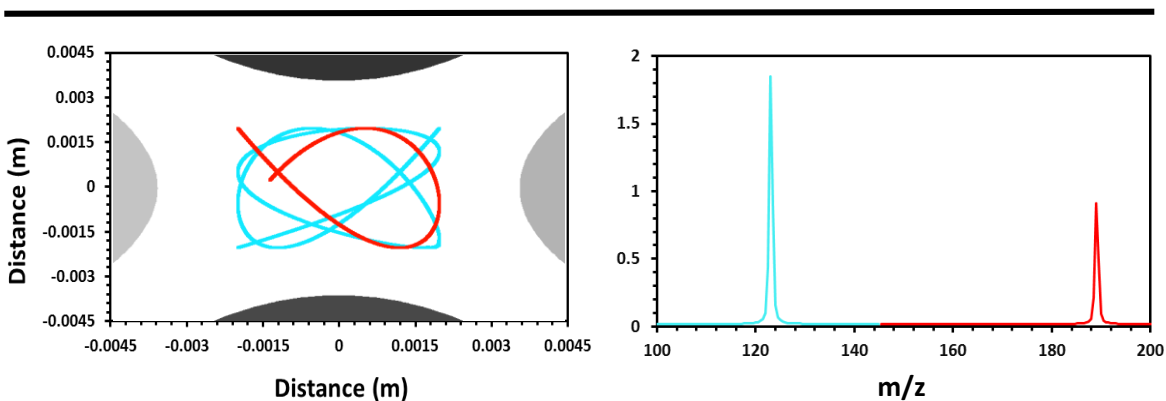

Figure 3. A simulation of three possible trajectories (left) for two different m/z trapped ions as well as the simulated mass spectrum (right) are shown above. The two blue trajectories represent the m/z 123 peak resulting in a doubled peak amplitude. The red trajectory represents the m/z 189 peak. This was determined using the following initial input parameters: a ring radius of 0.0036 meters, a time step of 1 x 10^{-13} seconds, 189 mass (amu) red, 123 mass (amu) blue, 8000 points, an alternating frequency of 140 kHz, an AC potential of 72 V, a DC potential of 2 V, initial velocity of x and z of 0 m/s, and an initial position of x and z of 0.002 m.

Further analysis can be implemented on the ions in question. The mass of the ions can be altered to observe how the mass affects the ion trajectories. Two ions with varying mass can be observed at the same time to compare ion paths side by side. The initial positions in the x and z directions can be altered to observe the changing orbitals, as well as the initial velocities in the x and z directions. **Figure 4** shows an example of the velocity distribution of a specific ion determined through the program.

Table 1. Program input variables for the velocity distribution.

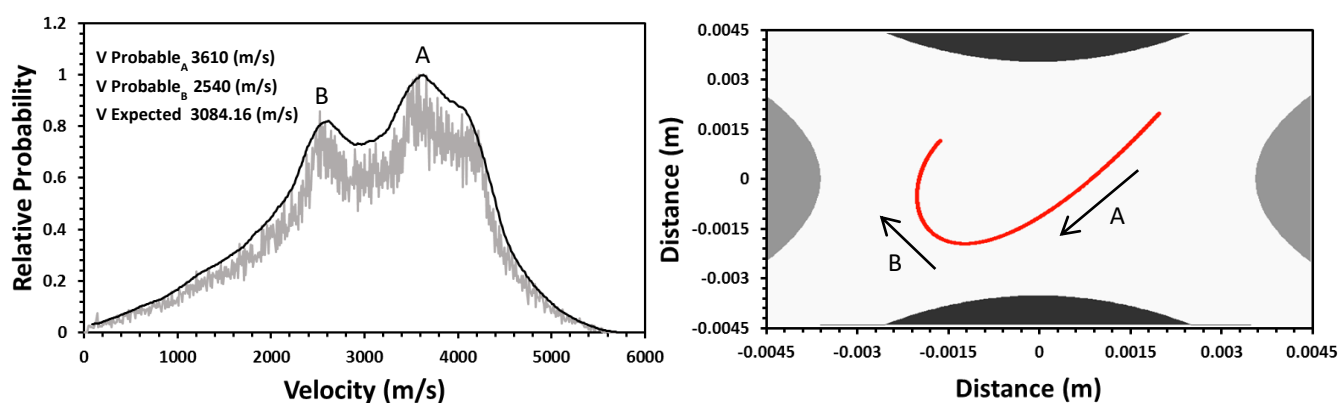| Input Variable	Input Value
Time Step(s)	1×10^{-12}
Points	3×10^{5}
Mass(amu)	182
Ring Radius(m)	0.0036
RF Frequency (kHz)	140
Bin Size	10
AC Voltage(V)	72
DC Voltage(V)	2
Initial Velocity (x,y,z)(m/s)	100
Initial Position (x,y,z)(m)	.002

Figure 4. The probability of the velocity of bis(cyclopentadienyl)chromium(II) in the trap over time (left) and the first 2500 points of the ion trajectory (right) are displayed above. The solid black line is the moving average spectrum; the grey line is the raw simulation. The most probable velocity can be determined from the maxima. Input parameters are shown in **Table 1**. The most probable and expected velocities are calculated from the raw simulation velocity data**.** The bimodal distribution creates the two most probable velocities for the charged ions located at V Probable$_A$ (A) and V Probable$_B$ (B), where V Probable$_A$ results from the ion being repelled away from an electrode and V Probable$_B$ results from the ion slowing down upon approaching the electrode forcing it to change directions.

From the most probable velocity, the most probable energy is calculated using the kinetic energy expression $\frac{1}{2}mv^2$. This energy will provide an idea of the energetics of the collisions occurring in the ion trap to verify the accuracy of the calibration curve energy assignments.
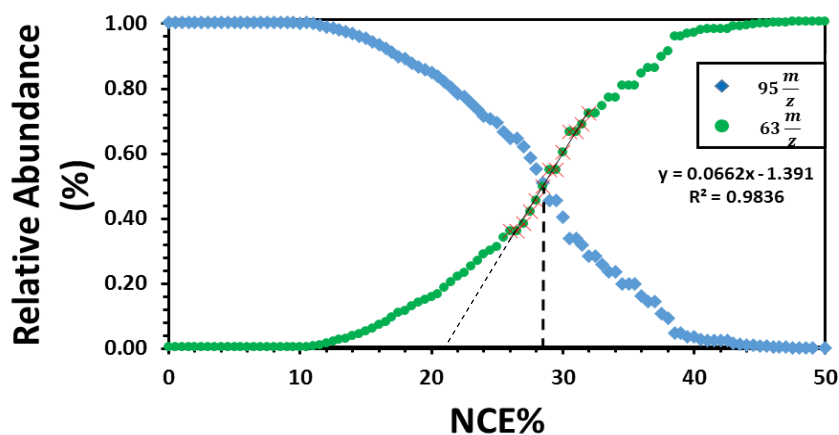
Results & Discussion

Figure 5. The experimentally measured relative abundance of the parent and fragment peak of Cu(MeOH)$^+$ when subjected to varying NCE % is represented above. The middle points of the fragment peak are fit with a linear function. The linear expression is used to solve for the NCE % at which the fragment peak is at 0.5 relative abundance. This NCE % is represented by the thick vertical dashed line. The smaller dashed line represents how previous publications have solved for the NCE %.[10]

Figure 5 demonstrates how increasing the NCE % affects the experimentally determined relative abundances of the parent and fragment molecules.[10] As the NCE % increases, the energy of collisions increases proportionally, leading to more fragmentation.[10] The sigmoidal curves generated were also observed by Zins et al. whilst approximating the enthalpies of fragmentations to further determine whether certain species could react in the interstellar medium. After the NCE % has been increased past a certain threshold, the parent molecule will no longer be observed.[10] The linear equation is fit to the fragment points where the fragment peak reaches 50% of its relative abundancy. This point lies near the intersection of the parent and fragment abundance curves.[10] The intersection between the two curves falling near the 50% fragment abundance point was also observed by Zins et al.[10] Previous publications assigned the x axis intersection of the line of best fit, appearance NCE %, a literature energy value to generate a calibration curve.[9,10] Based on the velocity distribution shown in **Figure 4**, the appearance NCE % would represent the tail end of this distribution or the highest energy collisions in the system. These would be the least probable collisions in the ion trap. To correct these inadequacies, the NCE % assigned correlates to when the fragment peak reaches half of its maximum relative abundance. The half maximum abundance correlates to 50% of the molecular collisions having an energy that is greater than or equal to the bonding energies between metal center and ligand/functional group. Once the NCE % of every molecule was experimentally determined, they are assigned known bond energies from

the literature and a calibration curve is generated, as shown in **Table 2** and **Figure 6**, respectively.

Table 2. The published energy values assigned the NCE %.

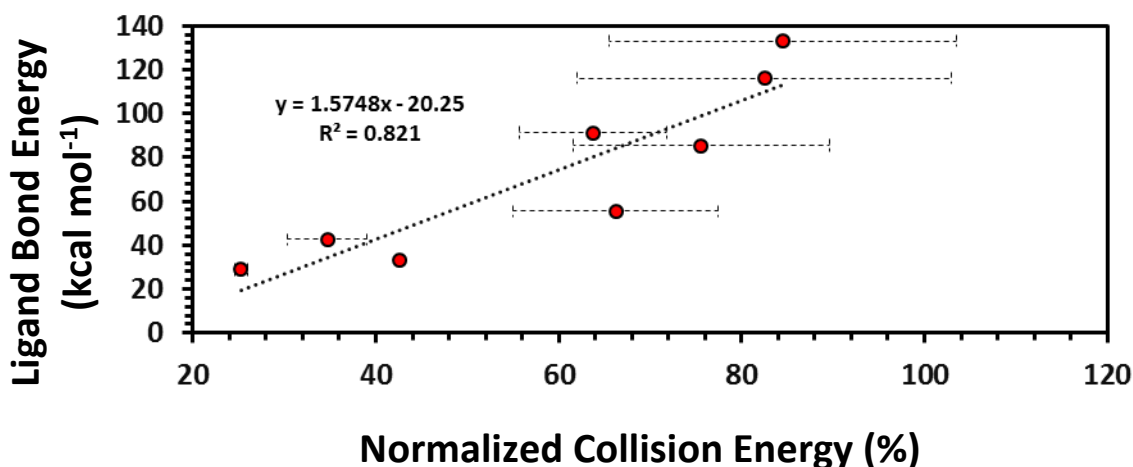| Complex	Fragment	NCE % Avg experimental	Ligand Bond E(kcal mol^{-1})
K$^+$(glycine)	K$^+$	25.2	28.90[12]
HGly$^+$	CH$_2$NH$_2$$^+$	42.6	33.20[13]
Cu$^+$(MeOH)	Cu$^+$	34.7	42.66[18]
Cr$^+$(C$_6$H$_6$)$_2$	Cr$^+$(C$_6$H$_6$)	66.3	55.40[14]
Fe$^+$(C$_5$H$_5$)$_2$	Fe(C$_5$H$_5$)$^+$	75.6	85.50[15]
Ni$^+$(C$_5$H$_5$)$_2$	Ni(C$_5$H$_5$)$^+$	63.8	91.30[16]
Cr$^+$(C$_5$H$_5$)$_2$	Cr(C$_5$H$_5$)$^+$	82.5	116.20[16]
Co$^+$(C$_5$H$_5$)$_2$	Co(C$_5$H$_5$)$^+$	84.5	133.10[16]

Figure 6. The calibration curve generated from **Table 2** with the equation and R^2 included is displayed above. As the bond energy increases, the NCE % required to break the bond increases as well. The error bars were determined by collecting three sets of data staying within the 64.2% confidence interval or $\pm$ one standard deviation.

Figure 6 represents the average NCE% with an assigned bond energy.[9] Three sets of data were taken for each molecule and averaged to provide the data point and error bars.[9] The standard deviation and error of each molecule increases with increasing energy and increasing NCE %.[9] Brodbelt and Colorado observed a similar trend: as the applied voltage increased, the standard deviation of their energy assignment increased as well.[9] This is further verified by the simulated energy distributions created, presented in **Figure 7**. It can be seen that as the energy of the collisions increase, the energy distributions broaden drastically. This is one explanation for the increased error bars with increasing NCE %. Increasing the NCE %

directly increases the voltage applied across the ion trap and thus increases the energy of collisions.[9] Depression of the standard deviation could have been achieved by having a more stable backing pressure of helium inside the ion trap itself. The calibration curve by itself is not enough, however. One of the major goals of this research was to provide a theoretical way to obtain energetics quickly through simulation. The voltage values of the ion trap were recorded for the experiment on bis(benzene)chromium(0), as **Table 1** shows, and several velocity distributions were simulated.[21] From these velocity probability distributions, collisional energy distributions were created and the relative abundance of the parent and fragment peaks were determined for varying AC voltage values.
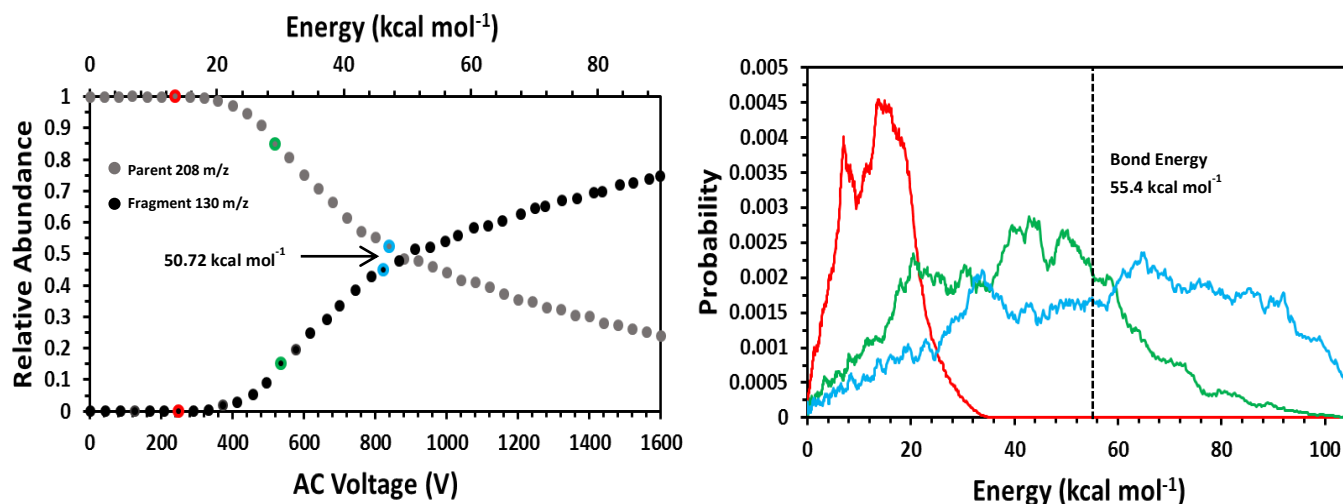

Figure 7. The simulated CID data for bis(benzene)chromium(0) is shown above. The fragment and parent ion abundances are plotted against varying AC voltage and energy (kcal mol^{-1}) (left). This yielded an expected bond energy of 50.72 kcal mol^{-1} at the intersection point. The energy distribution simulated is shown on the right along with the literature energy value of bis(benzene)chromium(0). The energy distributions were taken at certain points outlined on the abundance spectrum as red, green, and blue corresponding to each colored energy distribution respectively. From this, the accuracy of the simulation is verified and the experimental data can be compared.

Figure 7 displays the relative abundance of the parent and fragment molecules for set AC voltages with the most probable energy of collisions shown on the top x axis along with three corresponding collisional energy distributions. The AC potential range is consistent with previous simulations.[19,20] As the collisional energy increases, the gradient at which the relative abundances change decreases due to the broadening of the energy distributions. From this broadening, it can be concluded that the appearance NCE % assignment through the linear fit is indeed inaccurate. The relative abundances for the fragment and ion were calculated through equation (7) and (8) respectively.

$$A_{frag} = \frac{\sum_{Be}^{\infty} P(\langle E \rangle)}{\sum_{0}^{\infty} P(\langle E \rangle)} \tag{7}$$

$$A_{ion} = \frac{\sum_{0}^{Be} P(\langle E \rangle)}{\sum_{0}^{\infty} P(\langle E \rangle)} \tag{8}$$

Where Be is the bond energy of the parent molecule to the corresponding ligand/functional group in kcal mol^{-1}, $P(\langle E \rangle)$ represents the probability energy distribution. The most probable energy was determined from the expectation velocity calculated for in equation (9).

$$v_{exp} = 1.273 \sum_{i} \langle v \rangle * \frac{P(\langle v \rangle)}{\sum_{i} P(\langle v \rangle)} \tag{9}$$

The bounds of the summation are determined through the inputs of the Bin Generation program, v_{exp} is the expectation velocity in m/s, $\langle v \rangle$ is the velocity in m/s at every step i, and $P(\langle v \rangle)$ is the probability of a certain velocity at every step i. The expectation velocity also has a correction factor to convert from 2 to 3 dimensions derived from 2d to 3d Maxwell Boltzmann distribution. From the calculated expectation velocity, the energy of the ion is determined by equation (10).

$$E_{ionJ} = \frac{1}{2} m v_{exp}^{2} \tag{10}$$

In equation (10), m represents the mass of the ion in kilograms. The energy of collisions was determined by assuming stationary helium atoms.[22] This enables only the use of the expectation velocity in the collisional energy calculation. A completely inelastic collision was assumed where collision energy was spread evenly between all available degrees of freedom within each molecule, and the total energy of the collision was determined by equation (11).[22]

$$E_{collision} = E_{ionkcal} * \frac{1}{(N_{ion} + N_{Helium})} \tag{11}$$

N_{ion} and N_{Helium} are the number of the degrees of freedom the ion and helium atom possess respectively. This approximates solving for the point vibration for which most of the energy gets transferred to when the two gas particles collide.[22] The bond energy of bis(benzene)chromium(0) was determined to be 55.40 kcal/mole through collision-induced dissociation with xenon gas in guided ion beam mass spectrometry.[13] At the intersection point on the abundance graph, the most probable energy of collisions between ion and helium atom calculated was 50.72 kcal mol^{-1}. This calculation was repeated for the remaining molecules to further analyze the accuracy of the results shown in **Table 3**.

Table 3. The theoretical energetic values compared to literature energy values.

Complex	Theoretical (kcal mol^{-1})	Literature (kcal mol^{-1})
K^+(glycine)	25.29	28.90[12]
$HGly^+$	30.36	33.20[13]
Cu^+(MeOH)	39.35	42.66[18]
$Cr^+(C_6H_6)_2$	50.72	55.40[14]
$Fe^+(C_5H_5)_2$	78.66	85.50[15]
$Ni^+(C_5H_5)_2$	83.80	91.30[16]
$Cr^+(C_5H_5)_2$	108.41	116.20[16]
$Co^+(C_5H_5)_2$	122.60	133.10[16]

Comparing the theoretical energies to known bond energies yielded an average percent error of 8.5%. This discrepancy potentially arises from assuming stationary helium atoms. The uncertainty may also originate from assuming an even distribution of energy across all degrees of freedom in both particles participating in the collision. However, the low percent error value verifies the accuracy of the simulation and the accuracy of the energy assignment from experimental data. This, unfortunately, lends no insight into the actual voltage value at a given NCE % by itself but further analysis could lead to an expeditious way to understand the collisional energetics within the ion trap using the program provided.

Conclusion

We have quantified the energy of a seris of ion-neutral collisions within an ion trap mass spectrometer through computer simulation. Our reported metric is a more accurate description of the energy imparted on the parent molecule than previous works that assigned the appearance NCE % in the creation of the calibration curve relating NCE % to energy.[9,10] The NCE % at which the abundance of the fragment reaches 50% of its relative intensity is designated a literature energy value. The 50% point lies near the intersection between the parent and fragment's sigmoidal abundance curves, a fact also observed by Zins et al. At high enough collisional energies, the relative abundance of the parent molecule becomes undetectable and the parent ion remains unchanged.[9,10] A calibration curve was created using this new energy assignment. As the average energy of the collisions within the system increases, the uncertainty of the energy distribution increases proportionally. We theorize that a stable backing pressure of helium gas will decrease the experimental uncertainty of collisional energies but not totally eliminate it. The simulation was also tested against all of the experimental energy values determined through previous publications.[14] Bis-(benzene)chromium(0) was chosen to show an example calculation of how these energies are theoretically determined. The previous literature determined the bond energy between the metal center and benzene complex to be 55.40 kcal mol^{-1}.[14] The simulation calculated the most probable energy to be at 50.72 kcal mol^{-1}. Further calculations were carried out for the rest of the molecules as well. The average percent error between theoretical and actual energy values across all the molecules was determined to be 8.5%. While these assignments are not exact, they suggest a more accurate description of the collisional energetics than pervious works.[9,10]

The error within our calculations potentially arises from the assuming an even energetic distribution across all possible degrees of freedom.[21,22] It may also arise from assuming stationary helium gas molecules. Future works should analyze the voltage applied across the ion trap experimentally as the NCE % is increased. Investigation behind simulating the trajectories in three dimensions could also lead to unforeseen consequences that occur from two dimensional simulation. These further investigations could lead to an expedient method to understand the collisional energies within an ion trap. This would advance the functionality of the ion trap by providing insight into the energetics very rapidly making it a useful tool for any experimental chemist performing CID mass spectrometry experiments.

Acknowledgements

References

1. Lu, M.; Wang, H.; Wang, Z.; Xing-Fang, L.; Chris, X. L.; Identification of Reactive Cysteines in a Protein Using Arsenic Labeling and Collision-Induced Dissociation Tandem Mass Spectrometry. *Journal of Proteome Research* (2008), 7(8), 3080-3090.

2. Divito, E. B.; Davic, A. P.; Johnson, M. E.; Cascio M.; Electrospray Ionization and Collision Induced Dissociation Mass Spectrometry of Primary Fatty Acid Amides. *Journal of Analytical Chemistry* (2012), 84(5), 2388-2394.

3. Johnson, A. R.; Carlson, E. E.; Collision-Induced Dissociation Mass Spectrometry: A Powerful Tool for Natural Product Structure Elucidation. *Journal of Analytical Chemistry* (2015), 87(21), 10668-10678.

4. Reynolds, J. D.; Burn, J. L. E.; Boggess, B.; Cook K. D.; Woods, C.; Structural Characterization of Various Dirhodium Compounds Using Fast Atom Bombardment and Collision-Induced Dissociation Mass Spectrometry. *Journal of Inorganic Chemistry* (1993), 32(24), 5517-5521.

5. Snyder, D. T.; Fedick, P. W.; Cooks, R. G.; Multigenerational Collision-Induced Dissociation for Characterization of Oragnic Compounds. *Journal of Analytical Chemistry* (2016), 88(19), 9572-9581.

6. Zhang, W.; Quernheim, M.; Rader, H. J.; Mullen, K.; Collision-Induced Dissociation Ion Mobility Mass Spectrometry for the Elucidation of Unknown Structures in Strained

Polycyclic Aromatic Hydrocarbon Macrocycles. *Journal of Analytical Chemistry* (2016), 88(1), 952-959.

7. Wang, Z. C.; Cole, C. A.; Demarais N. J.; Snow, T. P.; Bierbaum, V. B.; Reactions of Azine Anions with Nitrogen and Oxygen Atoms: Implications for Titan's Upper Atmosphere and Interstellar Chemistry. *Journal of the American Chemical Society* (2015), 137(33), 10700-10709.

8. Cole, C. A.; Wehres, N.; Yang, Z.; Thomsen, D. L.; Snow, T. P.; Bierbaum V. M.; A Gas-Phase Formation Route to Interstellar Trans-Methyl Formate. *The American Astronomical Society* (2012), 745(1), 1-4.

9. Colorado, A.; Brodbelt, J.; An Empirical Approach to Estimation of Critical Energies by Using a Quadrupole Ion Trap. *Journal of the American Society for Mass Spectrometry* (1996), 7(11), 1116-1125.

10. Zins, E. L.; Primm, C.; Vettier, L.; Chabound, M.; Krim, L.; May Interstellar Leucine React with NO Radicals Present in Interstellar/Interplanetary Medium? An Ion-Trap Mass Spectrometry Study. *International Journal of Mass Spectrometry* (2013), 348, 47-52.

11. Guangxiang, W.; Graham, C.,; Zheng,O.; Meng, Y.; Chappell W. J.; Wolfgang, R. P.; Ion Trajectory Simulation for Electrode Configurations with Arbitrary Geometries. *Journal of the American Society for Mass Spectrometry* (2006), 17(9), 1216-1228.

12. Moision, R. M.; Armentrout, P.B.; An Experimental and Theoretical Dissection of Potassium Cation/Glycine Interactions. *Journal of Physical Chemistry Chemical Physics* (2004), 6, 2588-2599.

13. Armentrout, P. B.; Heaton, A. L.; Ye, S. J.; Thermodynamics and Mechanisms for Decomposition of Protonated Glycine and Its Protonated Dimer. *Journal of Physical Chemistry A* (2011), 115(41), 11144-11155.

14. Meyer, F.; Khan, F. A.; Armentrout, P.B.; Thermochemistry of Transition Metal Benzene Complexes: Binding Energies of $M(C_6H_6)_x$ + (x = 1,2) for M = Ti to Cu. *Journal of American Chemical Society* (1995), 117(38), 9740–9748.

15. Faulk, J.D.; Dunbar, R.C.; Photodissociation Spectroscopy of Gas-Phase Ferrocene Cation. *Journal of American Society for Mass Spectrometry* (1991), 2(2), 97-102.

16. Revesz, A.; Szepes, L.; Baer, T.; Sztaray, B.; Binding Energies and Isomerization in Metallocene Ions from Threshold Photoelectron Photoion Coincidence Spectroscopy. *Journal of the American Chemical Society* (2010), 132(50), 17795-17803.

17. More, M. B.; Ray, D.; Armentrout P. B.; Cation-Ether Complexes in the Gas Phase: Bond Dissociation Energies of M^+(dimethyl ether)$_x$, x = 1-3, M^+(1,2-dimethoxyethane)$_x$, x = 1 and

2, and M$^+$(12-crown-4) Where M = Rb and Cs. *Journal of Physical Chemistry A* (1997), 101(5), 7007-7017.

18. Yang, Z.; Rannulu, N. S.; Chu, Y.; Rodgers, M. T.; Bond Dissociation Energies and Equilibrium Structures of Cu$^+$ (MeOH)$_x$, x = 1-6, in the Gas Phase: Competition between Solvation of the Metal Ion and Hydrogen-Bonding Interactions. *Journal of Physical Chemistry A* (2008), 112(3), 388-401.

19. Li, A.; Higgs, J. M.; Austin D. E.; Chatoic motion of single ions in a toroidal ion trap mass analyzer. *International Journal of Mass Spectrometry* (2017), 421, 95-103.

20. Higgs, J. M.; Austin D. E.; Simulations of ion motion in tordial ion traps. *International Journal of Mass Spectrometry* (2014), 363, 40-51.

21. Zhao, X.; Krstic, P.; A molecular dynamics simulation study on trapping ions in a nanoscale Paul trap. *Nanotechnology* (2008), 19(19), 195702.

22. Plass, R., W.; Cooks, G. R.; A model for energy transfer in inelastic molecular collisions applicable at steady state or non-steady state and for an arbitrary distribution of collision energies. J*ournal of the American Society for Mass Spectrometry* (2003), 14(12), 1348 – 1359.